Original Article

MOLECULAR METABOLISM

Mitochondrial transcription factor B2 is essential for mitochondrial and cellular function in pancreatic β-cells

Lisa M. Nicholas [1,*,5], Bérengère Valtat [1,5], Anya Medina [1], Lotta Andersson [1], Mia Abels [2], Inês G. Mollet [3], Deepak Jain [4], Lena Eliasson [3], Nils Wierup [2], Malin Fex [1], Hindrik Mulder [1]

ABSTRACT

Objective: Insulin release from pancreatic β-cells is controlled by plasma glucose levels via mitochondrial fuel metabolism. Therefore, insulin secretion is critically dependent on mitochondrial DNA (mtDNA) and the genes it encodes. Mitochondrial transcription factor B2 (TFB2M) controls transcription of mitochondrial-encoded genes. However, its precise role in mitochondrial metabolism in pancreatic β-cells and, consequently, in insulin secretion remains unknown.

Methods: To elucidate the role of TFB2M in mitochondrial function and insulin secretion *in vitro* and *in vivo*, mice with a β-cell specific homozygous or heterozygous knockout of *Tfb2m* and rat clonal insulin-producing cells in which the gene was silenced were examined with an array of metabolic and functional assays.

Results: There was an effect of gene dosage on *Tfb2m* expression and function. Loss of *Tfb2m* led to diabetes due to disrupted transcription of mitochondrial DNA (mtDNA) and reduced mtDNA content. The ensuing mitochondrial dysfunction activated compensatory mechanisms aiming to limit cellular dysfunction and damage of β-cells. These processes included the mitochondrial unfolded protein response, mitophagy, and autophagy. Ultimately, however, these cell-protective systems were overridden, leading to mitochondrial dysfunction and activation of mitochondrial-dependent apoptotic pathways. In this way, β-cell function and mass were reduced. Together, these perturbations resulted in impaired insulin secretion, progressive hyperglycemia, and, ultimately, development of diabetes.

Conclusions: Loss of *Tfb2m* in pancreatic β-cells results in progressive mitochondrial dysfunction. Consequently, insulin secretion in response to metabolic stimuli is impaired and β-cell mass reduced. Our findings indicate that TFB2M plays an important functional role in pancreatic β-cells. Perturbations of its actions may lead to loss of functional β-cell mass, a hallmark of T2D.

Keywords Mitochondrial metabolism; Pancreatic β-cells; Insulin secretion

1. INTRODUCTION

Pancreatic β-cells maintain metabolic homeostasis by tightly coupling ambient glucose levels to insulin secretion [1,2]. In Type 2 Diabetes (T2D), which affects more than 380 million people globally [3], β-cell dysfunction and loss of β-cell mass lead to defective insulin secretion and development of diabetes [1,4]. Mitochondrial metabolism plays a central role in the glucose-sensing ability of β-cells via the process of stimulus-secretion coupling [5], therefore controlling insulin release from these cells [6].

mtDNA encodes 13 polypeptides that are part of the electron transport complexes I, III, IV, and V, which carry out cell respiration and ATP synthesis, also known as oxidative phosphorylation (OXPHOS) [7]. Both mitochondrial transcription factor A (TFAM) and mitochondrial transcription factor B2 (TFB2M) are required for the transcription of mitochondrial genes, whereas mitochondrial transcription factor B1 (TFB1M) acts as a translation factor for mitochondrial proteins [8,9]. Mice with a β-cell specific knockout (KO) of *Tfam* develop β-cell dysfunction and hyperglycemia [10]. Carriers of a common variant of the *TFB1M* gene (rs950994) exhibit reduced expression of *TFB1M* in pancreatic islets as well as impaired insulin response to glucose, elevated glucose levels during an oral glucose tolerance test, and increased future risk of T2D [11]. Mice with a β-cell specific KO of *Tfb1m* display mitochondrial dysfunction, reduced ATP production, and, consequently, impaired glucose-stimulated insulin secretion (GSIS) [12].

[1]Department of Clinical Sciences Malmö, Unit of Molecular Metabolism, Lund University Diabetes Centre, CRC, Skåne University Hospital, 20502, Malmö, Sweden [2]Department of Clinical Sciences Malmö, Unit of Neuroendocrine Cell Biology, Lund University Diabetes Centre, CRC, Skåne University Hospital, 20502, Malmö, Sweden [3]Department of Clinical Sciences Malmö, Unit of Islet Cell Exocytosis, Lund University Diabetes Centre, CRC, Skåne University Hospital, 20502, Malmö, Sweden [4]Deparment of Experimental Medical Science, Lund University Diabetes Centre, CRC, Skåne University Hospital, 20502, Malmö, Sweden

[5] Lisa M. Nicholas and Bérengère Valtat contributed equally to this work.

*Corresponding author. University of Cambridge Metabolic Research Laboratories, Wellcome Trust-MRC Institute of Metabolic Science, Addenbrooke's Hospital, Cambridge, CB2 0QQ, United Kingdom. E-mail: ln305@medschl.cam.ac.uk (L.M. Nicholas).

Received April 2, 2017 • Revision received May 6, 2017 • Accepted May 10, 2017 • Available online 19 May 2017

http://dx.doi.org/10.1016/j.molmet.2017.05.005

In contrast to TFAM and TFB1M, knowledge about the role of TFB2M in pancreatic β-cells and whether loss of TFB2M leads to mitochondrial dysfunction is lacking. To this end, we examined the functional consequences of *Tfb2m*-deficiciency in mice with a β-cell specific homozygous and heterozygous KO of *Tfb2m* and in rat clonal insulin-producing cells. We found that *Tfb2m*-deficiency rapidly led to widespread mitochondrial dysfunction, which gradually overrode cell-protective systems. This resulted in β-cell dysfunction, as well as increased activation of apoptosis via the mitochondrial-dependent pathway and loss of β-cell mass.

2. MATERIALS AND METHODS

2.1. Generation of mice with a β-cell specific homozygous and heterozygous knockout of *Tfb2m*

To generate a conditional KO of *Tfb2m* in β-cells, we used $Tfb2m^{loxP/loxP}$ mice in which exon 2 of the *Tfb2m* locus was flanked by two loxP sites. Sperm to establish our colony of these mice was obtained from the Knock Out Mouse Project (https://www.komp.org/index.php) at University of California, Davis. Heterozygous $Tfb2m^{+/loxP}$ mice were mated to heterozygous transgenic mice expressing *Cre* recombinase under the control of Rat insulin 2 gene promoter (*Rip-Cre*) [13]. Mice with the genotype $Tfb2m^{+/loxP}$, $^{+/Rip\text{-}Cre}$ were recovered from this cross and bred with $Tfb2m^{loxP/loxP}$ mice to generate $Tfb2m^{loxP/loxP}$, $^{+/Rip\text{-}Cre}$ (β-$Tfb2m^{-/-}$) β-cell-specific *Tfb2m* homozygous KO mice, $Tfb2m^{+/loxP}$, $^{+/Rip\text{-}Cre}$ (β-$Tfb2m^{+/-}$) β-cell-specific *Tfb2m* heterozygous KO mice, and $Tfb2m^{loxP/loxP}$ control mice. Both male and female animals were used for the experiments in control and β-$Tfb2m^{-/-}$ 18-50-day-old mice; only males were used for experiments in control and β-$Tfb2m^{+/-}$ mice at six to seven months of age. The breeding and handling of mice were carried out according to procedures approved by the regional animal ethics committee in Lund, Sweden.

2.2. Glucose and insulin measurements

Blood was collected when the mice were killed by cervical dislocation and decapitation at d18, d50 (β-$Tfb2m^{-/-}$), and seven months of age (β-$Tfb2m^{+/-}$). Quantitative determination of plasma glucose was carried out using Infinity™ Glucose Oxidase (Thermo Fisher Scientific, (Waltham, MA, USA). Insulin was measured by enzyme-linked immunosorbent assay (ELISA) (Mercodia, Uppsala, Sweden). Intravenous glucose tolerance test (IVGTT) was also carried out on β-$Tfb2m^{+/-}$ mice at six months of age as described [15]. Food was removed 1 h before the glucose challenge. The mice were anesthetized as previously described [15]. Blood was collected retro-orbitally at 0, 1, 5, 10, 20, 50 and 75 min after intravenous injection of glucose (1 g/kg body weight) for determination of plasma glucose and insulin concentration as described above.

2.3. Isolation of pancreatic islets

The pancreas was perfused with Collagenase P solution (Roche) (35 day old and adult mice: 3 ml; 18 day old mice: 1 ml) through the common bile duct. Pancreata were harvested and digested at 37 °C for 18 min (35 day old and adult mice) or 15 min (18 day old mice). Islets were hand-picked under a stereo microscope and incubated at 37 °C overnight in a humidified atmosphere of air and 5% CO_2 in RPMI-1640 medium (11.1 mM glucose) supplemented with 10% FBS, 100 U/ml penicillin, and 100 μg/ml streptomycin sulfate.

2.4. Insulin secretion assay in islets

Islets were incubated in Krebs—Ringer bicarbonate buffer (KRBB) with 2.8 mM glucose for 1 h. Next, groups of islets were incubated for 1 h in KRBB containing 2.8 mM glucose, 16.7 mM glucose, 2.8 mM glucose, and 10 mM α-KIC or 2.8 mM glucose and 35 mM KCl. Secreted insulin was determined using ELISA (Mercodia, Uppsala, Sweden).

2.5. Islet insulin content

Insulin was extracted in 100 μl of ethanol/hydrochloric acid. The supernatant was assayed by ELISA (Mercodia, Uppsala, Sweden).

2.6. Mitochondrial membrane potential

Islets were loaded with 400 nM TMRM for 2 h in KRBB containing 2.8 mM glucose, permitting analysis in "quench mode" [16]. TMRM was excited at 543 nm, and emission detected with a 585 nm long-pass filter. Islets were stimulated with 16.7 mM glucose to investigate changes in mitochondrial membrane potential.

2.7. Tissue processing

Pancreata were dissected out and weighed before they were fixed overnight at 4 °C in Stefanini's solution. The tissue was washed thoroughly in Tyrode's solution containing 10% sucrose and then frozen on dry ice. 10 μm sections were cut and thaw-mounted on slides.

2.8. Immunohistochemistry

Sections were incubated with primary antibody against insulin (dilution: 1:5000, code: 9003, EuroDiagnostica, Malmö, Sweden) and with secondary antibody with specificity for guinea pig IgG (Jackson, West Grove, PA USA). Sections were mounted in PBS:glycerol (1:1).

2.9. Morphometry

For β-cell mass quantification, all islets in randomly selected parts of each pancreas were analyzed using NIS-Elements software (NIS-Elements 3.1, Nikon, Tokyo, Japan) as previously described [12]. Total insulin stained area and total section area were analyzed and calculated. The ratio achieved was multiplied with the pancreas weight to calculate the β-cell mass.

2.10. Transmission electron microscopy

Groups of 40—50 isolated islets were fixed in Millonig's buffer and postfixed in 1.0% osmium tetroxide then dehydrated and embedded in AGAR 100 (Oxfors Instruments Nordiska AB, Sweden). 70—90 nm thick ultrathin sections were cut, mounted, and contrasted before being examined in JEM 1230 electron microscope (JEOL-USA, Inc, MA, USA). Micrographs were analyzed with respect to mitochondrial morphology and granule distribution in relation to the cell membrane. Granule diameters were analyzed using ImageJ (NIH, freeware) and the 3D granule diameter was estimated [17]. The volume granule density (N_v) and surface density (N_s) were calculated from cell area and granule distance from membrane using an in-house Matlab program on MatLab7 (MathWorks, Natick, MA, USA) and volumetric methods described elsewhere [18].

2.11. Cell culture and RNA interference

INS-1 832/13 cells were cultured as previously described [19] and transfected using a mixture of Lipofectamine™ RNAiMAX Transfection Reagent (Invitrogen, Life Technologies, Stockholm, Sweden) and the respective Silencer® Select siRNAs. The control sequence, Silencer® Negative Control #2 (Ambion, Life Technologies) was employed. Cells were cultured in complete RPMI-1640 medium for 72 h at 37 °C, 5% CO_2 in the presence of 50 nM siRNA prior to functional analyses.

2.12. Insulin secretion assay in INS-1 832/13 cells

Prior to assay, cells were incubated in secretion assay buffer (SAB) and supplemented with 2.8 mM glucose for 2 h. Fresh buffer was then

added and cells were incubated for 1 h in SAB containing 2.8 mM glucose, 16.7 mM glucose, 10 mM pyruvate, 2.8 mM glucose and 35 mM KCl or 10 mM leucine/glutamine. Secreted insulin was determined by Coat-a-Count radioimmunoassay (Siemens Medical Solutions Diagnostics, Los Angeles, CA).

2.13. Quantification of mRNA expression using quantitative real-time-PCR (qRT-PCR)

Total RNA was extracted from islets and INS-1 832/13 cells using RNAeasy RNA purification kit (Qiagen GmbH, Hilden, Germany). Equal quantities of total RNA were reverse transcribed using RevertAid™ First-Strand cDNA synthesis kit (Fermentas, Vilnius, Lithuania). qRT-PCR was performed on ViiA7 qRT-PCR system, using predesigned TaqMan Gene Expression assays (PE Applied Biosystems, Foster City, CA, USA). Gene expression was determined by the absolute quantification method and normalized to the expression of *Hprt*.

2.14. Quantification of protein abundance using Western blotting

Islets (control, $n = 6$ mice and β-*Tfb2m*$^{-/-}$, $n = 5$ mice) and INS-1 832/13 cells ($n = 5$ different passages/group) were lysed in radioimmunoprecipitation assay buffer (RIPA) mixed with 1:100 (v/v) protease inhibitor cocktail (Sigma, St. Louis, MO, USA) and separated on a Mini-PROTEAN® TGX Precast Gel Any kDa (Bio-Rad, Hercules, CA, USA). Every gel was loaded with protein from all control and *Tfb2m*-deficient samples. For INS-1 832/13 cells, an equal amount of protein (20 μg) was loaded in each well. In contrast, due to the low protein yield in islets, wells were loaded with the maximum amount of protein available, which resulted in different amounts of protein loaded between control and β-*Tfb2m*$^{-/-}$ samples. Proteins were transferred to polyvinylidene diflouride membrane, using the TransBlot® Turbo™ Transfer System (Bio-Rad, Hercules, CA, USA), blocked and incubated overnight at 4 °C with primary antisera raised against: AKT, phospho-AKT (Ser 473), BAX, BCL-2, cleaved-caspase 3 (CC3), cleaved-caspase 9 (CC9), and DDIT3/CHOP (Cell Signaling Technology, Danvers, USA), HSP60, MT-ND1, PARKIN, PINK1, NDUFB8, SDHB, UQCRC2, MT-CO1, and ATP5A (total OXPHOS), TFAM, TFB1M, TFB2M (Abcam, Cambridge, UK), CLPP (Santa Cruz Biotechnology, Santa Cruz, USA). Membranes were washed and bound antibody detected using horseradish peroxidase-conjugated secondary antibodies and enhanced chemiluminescence reagents (Bio-Rad, Hercules, CA, USA). Image Lab software version 5.2.1 (Bio-Rad, Hercules, CA, USA) was used to quantify the density of specific bands. The abundance of proteins of interest is expressed relative to the abundance of β-tubulin (Abcam). All membranes were stripped once using Restore™ Western Blot Stripping Buffer (Thermo Fisher Scientific, Waltham, MA, USA) after detection of protein of interest in order to quantify the abundance of β-tubulin on the same membrane.

2.15. Immunofluorescence

Dispersed islets and INS-1 832/13 cells were cultured for 24 h. LC3B-GFP (Premo Autophagy sensors BacMam 2.0; Life technologies™, Waltham, MA, USA) was added to cells and cultured for 18 h. Two hours prior to end of incubation time, LysoTracker® Red DND-99 or Mitotracker® Mitochondrion-selective Probe (Life technologies™) diluted in fresh RPMI medium was added. Cells were washed in PBS and fixed with 4% paraformaldehyde for 20 min. Cells were co-stained with Polyclonal Guinea pig Anti-insulin (Dako, Carpinteria, CA, USA), using Alexa Fluor 594 anti-guinea pig IgG (H + L) conjugate (Invitrogen, Waltham, MA, USA) as a secondary antibody. Finally, cells were mounted with Vectashield mount with DAPI for nuclear morphology (Vector Laboratories, CA, USA). Images of cells in the 8 well slide chambers, viewed by an epi-fluorescence microscope (Olympus, BX60) with a 100× objective, were captured with a digital camera (Nikon DS-2Mv). Image data were collected with an ArrayScan™ XTI Live High Content Platform with a 20× objective (Cellomics, Waltham, MA, USA). Images of 500 cells for each treatment group were analyzed to obtain LC3 fluorescence area per cell.

2.16. Mitochondrial DNA content

Genomic and mitochondrial DNA was extracted and amplified by PCR, using primers for melanocortin-4 receptor (MC4R) and cytochrome oxidase subunit II (CoxII), respectively.

2.17. Quantification of ATP content

Islets and INS-1 832/13 cells were incubated in SAB containing 2.8 or 16.7 mM glucose for 1 h and stimulated. Islets and cells were lysed followed by flash-freezing in a mixture of dry-ice and ethanol. The content of ATP at 2.8 or 16.7 mM glucose was assayed using a luciferase-based luminescent assay (BioTherma, Handen, Sweden) according to the manufacturer's instructions.

2.18. Citrate synthase activity

Citrate synthase activity was measured in isolated mitochondria from INS-1 832/13 cells. Activity was determined at 412 nm by adding 10 mM oxaloacetic acid and detecting the formation of 2-nitro-5-thiobenzoic acid as previously described [20].

2.19. Oxygen consumption

Oxygen consumption rates (OCR) were measured by the XF24 Extracellular Flux Analyzer (Seahorse Bioscience, North Billerica, MA). Cells were pre-incubated for 2 h at 37 °C in assay buffer containing 2.8 mM glucose. Respiration was measured in the presence of 16.7 mM glucose. Oligomycin, FCCP and rotenone were injected as previously shown [21]. All calculations were done as previously described [21].

2.20. Detection of ROS

Reactive oxygen species (ROS) were detected in the presence and absence of 10 μM of the antioxidant N-acetyl-L-cysteine using the DCFDA — Cellular ROS Detection Assay Kit (Abcam, Cambridge, UK) according to the manufacturer's instructions.

2.21. Statistics

All calculations were performed in GraphPad Prism 6.03 (GraphPad, La Jolla, California, USA) software. *P* values were considered significant at less than 0.05. All data are presented as mean ± SEM of the indicated number of experiments or animals. Data were analyzed using unpaired Student's *t*-test, 1-way ANOVA or repeated measure of 2-way ANOVA with Tukey's test post hoc when more than two groups were compared.

3. RESULTS

3.1. Loss of *Tfb2m* in β-cells results in disrupted glucose homeostasis and development of diabetes

Mice with a homozygous KO of *Tfb2m* in β-cells (β-*Tfb2m*$^{-/-}$) exhibited increased plasma glucose ($P < 0.05$; Figure 1A) but no change in plasma insulin concentration (Figure 1B) in the freely-fed state as early as 18 days of age. At 50 days of age, hyperglycemia was further exaggerated in β-*Tfb2m*$^{-/-}$ mice ($P < 0.0001$; 1c); plasma insulin levels were now markedly reduced in the freely-fed state ($P < 0.01$; Figure 1D).

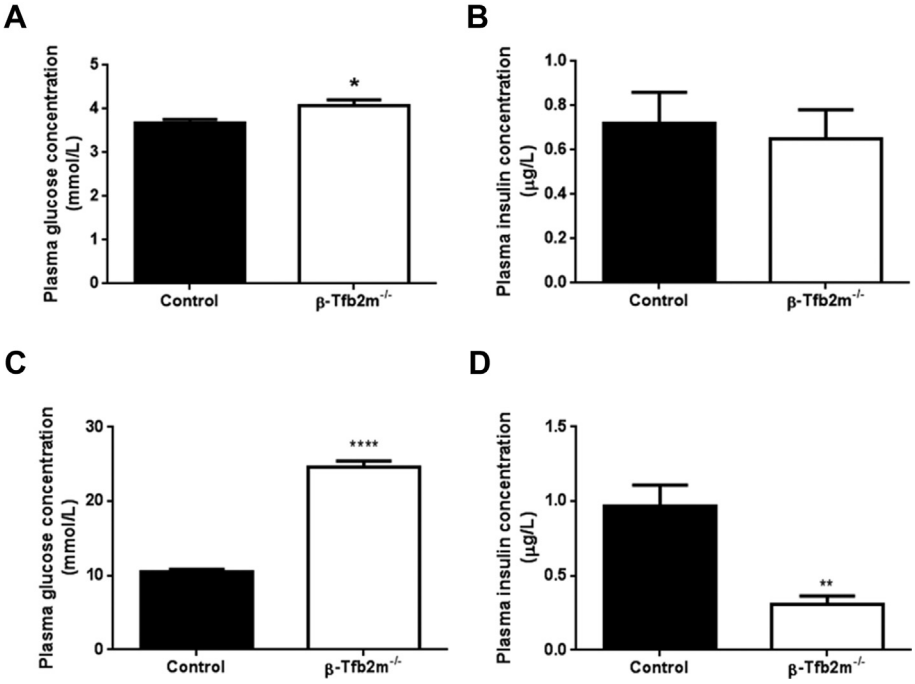

Figure 1: Glucose homeostasis in control and β-*Tfb2m*$^{-/-}$ mice. (A) Plasma glucose and (B) insulin concentrations in non-fasted control and β-*Tfb1m*$^{-/-}$ mice at 18 days of age; control, $n = 11$ and β-*Tfb1m*$^{-/-}$, $n = 13$. (C) Plasma glucose and (D) insulin concentrations in non-fasted control and β-*Tfb1m*$^{-/-}$ mice at seven weeks of age; control, $n = 7$ and β-*Tfb1m*$^{-/-}$, $n = 6$. All data are mean ± s.e.m. Statistical differences were examined by unpaired Student's *t*-test. *P < 0.05, **P < 0.01 and ****P < 0.0001 versus the corresponding value for control mice.

3.2. Loss of *Tfb2m* in β-cells results in decreased expression of mitochondrial encoded genes in pancreatic islets

We next examined whether the diabetic phenotype of β-*Tfb2m*$^{-/-}$ mice was due to decreased expression of mitochondrial-encoded genes. *Tfb2m* mRNA expression was reduced by about 80% in islets of β-*Tfb2m*$^{-/-}$ mice (at 35 days of age) (P < 0.01; Figure 2A). While mRNA expression of *Tfam* was decreased (P < 0.05), TFAM protein abundance was unchanged (Figure 2B). In contrast, *Tfb1m* gene expression was unaffected by loss of β-*Tfb2m* (Control: 1.02 ± 0.13; β-*Tfb2m*$^{-/-}$: 0.94 ± 0.06). There was a significant reduction in the expression of mitochondrial-encoded genes *mt-Atp8* (P < 0.001), *mt-Co1* (P < 0.01), *mt-Cyb* (P < 0.05), *mt-Nd1* (P < 0.05), and *mt-Rnr2* (P < 0.05), as well as protein abundance of MT-CO1 (P < 0.05) in β-*Tfb2m*$^{-/-}$ islets (Figure 2C,D). There was also decreased abundance of nuclear-encoded mitochondrial proteins NDUFB8 (P < 0.05) and UQCRC2 (P < 0.05) and increased ATP5A (P < 0.05) abundance, which are part of Complex I, III, and V, respectively (Figure 2D). This suggests that the stability of nuclear encoded proteins in mitochondria depends on critical mitochondrial-encoded proteins [12]. mtDNA content was also decreased in β-*Tfb2m*$^{-/-}$ islets (Figure 2E).

3.3. Loss of *Tfb2m* in β-cells leads to mitochondrial dysfunction and consequently impaired insulin secretion

Next, we determined the functional consequences of β-cell specific loss of *Tfb2m* in islets. A critical determinant of mitochondrial function is glucose-induced hyperpolarization of the inner mitochondrial membrane, which drives the respiratory chain. Indeed, the maximal decrease in TMRM fluorescence was reduced by 40% in islets from β-*Tfb2m*$^{-/-}$ mice after stimulation with 16.7 mM glucose (Day 18; P < 0.05, Figure 3A).

Given mitochondrial dysfunction in β-*Tfb2m*$^{-/-}$ islets and the regulatory role of mitochondria in insulin secretion, we next investigated GSIS *ex vivo* in isolated pancreatic islets. GSIS was already compromised in β-*Tfb2m*$^{-/-}$ mice at 18 days of age (P < 0.001) and this persisted after weaning (Day 35; P < 0.001) (Figure 3B,C). We also examined insulin secretion in response to the mitochondrial fuel α-ketoisocaproic acid (α-KIC), as well as potassium chloride (KCl), which bypasses metabolic coupling and directly depolarizes the plasma membrane. α-KIC-stimulated insulin secretion was impaired in islets from β-*Tfb2m*$^{-/-}$ mice at both 18 (P < 0.05; Figure 3B) and 35 days of age (P = 0.06; Figure 3C). In contrast, KCl-stimulated insulin secretion was not affected in β-*Tfb2m*$^{-/-}$ islets before as well as after weaning (Figure 3B,C). Islet insulin content was unchanged in β-*Tfb2m*$^{-/-}$ mice at 18 days of age (Control: 9.4 ± 2.7 μg/islet vs. β-*Tfb2m*$^{-/-}$: 7.9 ± 2.0 μg/islet).

Since we observed perturbed GSIS in β-*Tfb2m*$^{-/-}$ islets, we next examined granule ultrastructure. β-cells in β-*Tfb2m*$^{-/-}$ islets from 18 day old mice displayed increased surface density of docked large dense core vesicles (LDCV) in which insulin is packaged (P < 0.05; Figure 3D). However, volume density of LDCV, which reflects total number of insulin granules, was unaltered (Control: 8.16 ± 0.31 granules/μm^3 vs. β-*Tfb2m*$^{-/-}$: 7.97 ± 0.33 granules/μm^3). These data are in line with our finding that insulin content is unchanged in β-*Tfb2m*$^{-/-}$ islets; an increased number of docked granules agrees with a deficiency of metabolic signals promoting exocytosis. Together, our data suggest that loss of *Tfb2m* leads to impaired mitochondrial function and metabolic coupling of insulin secretion.

3.4. Loss of *Tfb2m* in β-cells leads to altered mitochondrial ultrastructure and impaired mitophagy

In view of the mitochondrial dysfunction, we examined mitochondrial ultrastructure in β-*Tfb2m*$^{-/-}$ islets, using transmission electron microscopy (TEM). Indeed, there was an increased abundance of vesicular and swollen mitochondria in β-cells from *Tfb2m*-deficient mice (P < 0.0001; Figure 4A).

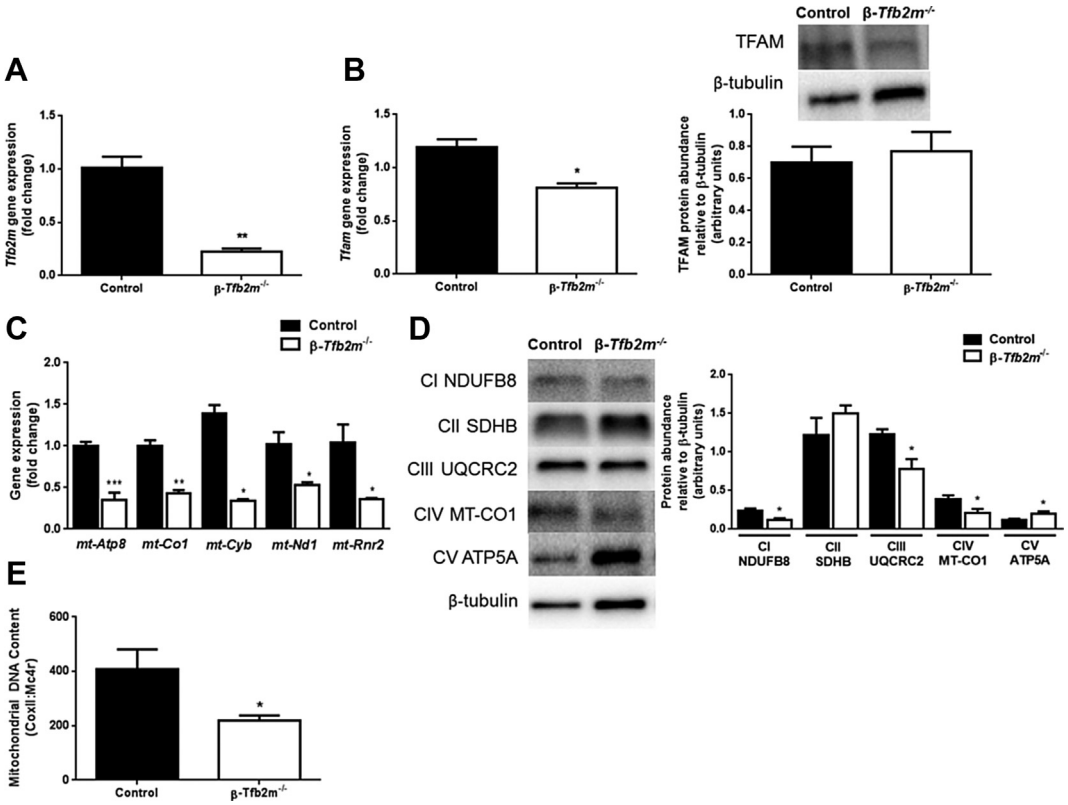

Figure 2: Expression of mitochondrial-associated genes and mitochondrial DNA content in control and β-*Tfb2m*$^{-/-}$ mice. (A) qRT-PCR analysis of *Tfb2m* mRNA in islets from control and β-*Tfb2m*$^{-/-}$ mice; $n = 3$ mice. (B) qRT-PCR analysis of *Tfam* mRNA (left; $n = 3$ mice/group) and western blot and densitometry analysis of TFAM protein abundance (right; control, $n = 6$ mice and β-*Tfb2m*$^{-/-}$, $n = 5$ mice) in islets from control and β-*Tfb2m*$^{-/-}$ mice. (C) qRT-PCR analysis of *Atp8*, *Co1*, *Cyb*, *Nd1*, and *Rnr2* mRNA in islets from control and β-*Tfb2m*$^{-/-}$ mice, $n = 3$ mice/group. (D) Western blot and densitometry analysis of NDUFB8, SDHB, UQCRC2, MT-CO1, and ATP5A protein abundance in in islets from control and β-*Tfb2m*$^{-/-}$ mice; control, $n = 6$ mice and β-*Tfb2m*$^{-/-}$, $n = 5$ mice. (E) Mitochondrial DNA content in islets from control and β-*Tfb2m*$^{-/-}$ mice; control, $n = 6$ mice and β-*Tfb2m*$^{-/-}$, $n = 9$ mice. Representative images for quantitative western blots are shown. All data are mean ± s.e.m. Statistical differences were examined by unpaired Student's *t*-test. *P < 0.05, **P < 0.01 and ***P < 0.001 versus the corresponding value for control mice.

We then assessed whether dysfunctional mitochondria were being effectively cleared by mitophagy, the selective degradation of mitochondria by autophagy. Autophagy is initiated by the formation of a double-membrane structure, the phagophore, which evolves into the autophagosome. Loss of *Tfb2m* in β-cells from β-*Tfb2m*$^{-/-}$ islets increased the number of mitochondria targeted to LC3-GFP-labeled autophagosomes (P < 0.05; Figure 4B). This raises two possibilities: (1) increased production of autophagosomes and/or (2) reduced clearance of autophagosomes due to impaired autophagosome-lysosome fusion [22].

To resolve this, we examined expression of the key mitophagy genes. *Pink1* (Control: 1.01 ± 0.09; β-*Tfb2m*$^{-/-}$: 1.12 ± 0.17), *Park2* (Control: 1.04 ± 0.20; β-*Tfb2m*$^{-/-}$: 0.93 ± 0.04), and *Mfn2* (Control: 1.01 ± 0.11; β-*Tfb2m*$^{-/-}$: 0.80 ± 0.08), which are involved in processes upstream of autophagosome formation [23], were unchanged in *Tfb2m*-deficient β-cells. Interestingly, expression of the master regulator of the β-cell, *Pdx1* (P < 0.01), which has recently been implicated in regulation of mitophagy in β-cells [22], was reduced in β-*Tfb2m*$^{-/-}$ islets, as was expression of gene targets downstream of *Pdx1*: *Ins1* (P < 0.05), *Ins2* (P < 0.01), *Slc2a2* (P < 0.001) (Figure 4C), and *Tfam* (P < 0.05; Figure 2B).

3.5. Loss of *Tfb2m* in β-cells leads to impaired autophagy

Based on our findings of increased density of docked LDCV in the face of reduced glucose- and α-KIC-stimulated insulin secretion, we investigated whether autophagic processes, which are responsible for clearing β-granules, were activated [24]. Immunostaining revealed an increased area of LC3^{+} puncta in β-cells from β-*Tfb2m*$^{-/-}$ islets at day 18 (P < 0.001; Figure 5A). This is characteristic of activation of autophagy and, accordingly, expression of the later-stage autophagy marker *Ctsb* [24] was increased (P < 0.05), while expression of *Lamp2*, a negative regulator of autophagy [25] was decreased (P < 0.05) (Figure 5B).

We determined autophagosome-lysosome fusion by quantifying the area of LC3^{+} puncta co-stained with the lysosome-specific dye Lysotracker, reflecting the presence of autophagolysosomes. This was disrupted in β-cells from β-*Tfb2m*$^{-/-}$ islets since there was a reduction in the number of LC3^{+} puncta co-stained with Lysotracker (P < 0.001; Figure 5C). Autophagy is also activated in response to ER stress [26]. Indeed, expression of the ER stress markers *Ddit3* (P < 0.0001) and *Cebpb* (P < 0.001) was significantly increased in β-*Tfb2m*$^{-/-}$ islets already at 18 days of age (Figure 5D).

3.6. Loss of *Tfb2m* in β-cells results in changes in apoptotic markers, reduced β-cell mass and reduced islet density

Dysregulated autophagy (including mitophagy) may eventually to lead to increased apoptosis. Accordingly, we found increased protein abundance of cleaved-caspase 9 (P < 0.05) but not cleaved-caspase 3 in β-*Tfb2m*$^{-/-}$ islets. The ratio of pro-apoptotic Bax to anti-apoptotic Bcl-2, however, was reduced (P < 0.05; Figure S1a), suggesting that protective mechanisms may be activated in these young β-*Tfb2m*$^{-/-}$ mice.

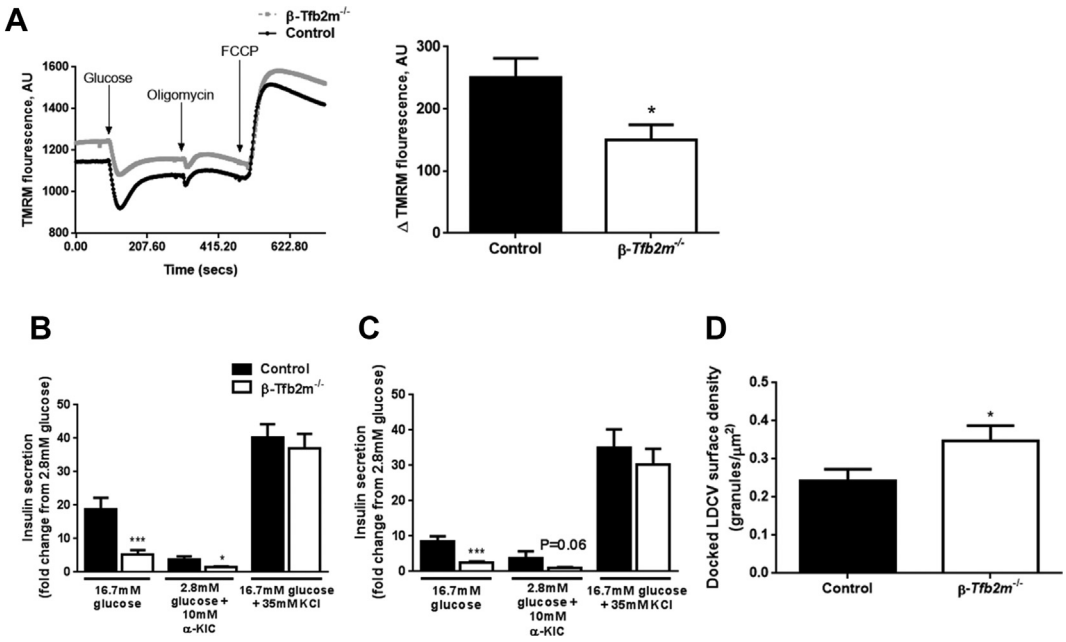

Figure 3: Loss of *Tfb2m* in β-cells leads to mitochondrial dysfunction and impaired insulin secretion. (A) Left – Kinetics of TMRM quenching in islets from control and β-*Tfb2m*$^{-/-}$ mice, $n = 5$ mice. Right – Change in TMRM fluorescence intensity from baseline following stimulation of isolated islets from control and β-*Tfb2m*$^{-/-}$ mice with 16.7 mM glucose, which leads to membrane hyperpolarization and minimal fluorescence intensity in quench mode, $n = 5$ mice. (B) Insulin secretion from islets isolated from control and β-*Tfb2m*$^{-/-}$ mice at 18 days of age. Islets were incubated for 1 h in 2.8 mM and 16.7 mM glucose, 2.8 mM glucose with 10 mM α-ketoisocaproic acid (α-KIC), and 16.7 mM glucose with 35 mM potassium chloride (KCl); control, $n = 5$ mice, β-*Tfb2m*$^{-/-}$, $n = 7$ mice. (C) Insulin secretion from islets isolated from control and β-*Tfb2m*$^{-/-}$ mice at 35 days of age. Islets were incubated for 1 h in 2.8 mM and 16.7 mM glucose, 10 mM α-ketoisocaproic acid (α-KIC), and 16.7 mM glucose with 35 mM potassium chloride (KCl); control, $n = 3$ mice, β-*Tfb2m*$^{-/-}$, $n = 6$ mice. (D) Surface density of docked large dense core vesicles in β-cells from control and β-*Tfb2m*$^{-/-}$ islets isolated from 18 day old mice. Granules were defined as docked if the center of the granules was within 150 nm of the plasma membrane, control and β-*Tfb2m*$^{-/-}$, $n = 4$ mice each at 18 days of age. All data are mean ± s.e.m. Statistical differences were examined by unpaired Student's *t*-test. *P < 0.05 and ***P < 0.001 versus the corresponding value for control mice.

In view of these findings, we examined whether there was loss of β-cell mass in seven week old *Tfb2m*$^{-/-}$ mice, which exhibit manifest diabetes. Indeed, unbiased quantitative stereological analysis showed a marked reduction in β-cell mass in diabetic β-*Tfb2m*$^{-/-}$ mice (P < 0.05; Figure S1b) as well as reduced islet density (P < 0.01; Figure S1c).

3.7. Heterozygous loss of *Tfb2m* in β-cells also results in disrupted glucose homeostasis in mice as a consequence of impaired mitochondrial function and diminished insulin secretion

Next, we determined whether *Tfb2m* exerts a gene dosage effect on islet function, using mice with one targeted *Tfb2m*-allele in β-cells (β-*Tfb2m*$^{+/-}$ mice). *Tfb2m* expression in β-*Tfb2m*$^{+/-}$ islets was reduced by about 50% compared to controls (P < 0.05; Figure S2a), confirming that *Tfb2m* expression depends on the number of functional alleles, i.e., gene dosage. In contrast to β-*Tfb2m*$^{-/-}$ mice, expression of *Tfam* was unchanged in β-*Tfb2m*$^{+/-}$ islets (Figure S2a), as was *Tfb1m* gene expression (Control: 1.02 ± 0.13; β-*Tfb2m*$^{+/-}$: 1.02 ± 0.10). Furthermore, of mitochondrial-encoded genes, only expression of *mt-Atp8* (P < 0.01) and *mt-Nd5/6* (P < 0.05) was decreased in islets of β-*Tfb2m*$^{+/-}$ mice; gene expression of *mt-Co1*, *mt-Cyb*, and *mt-Nd1* remained unchanged (Figure S2b).

In agreement with the more modest effect on mitochondrial proteins, the phenotype of β-*Tfb2m*$^{+/-}$ mice was delayed and less pronounced than that of β-*Tfb2m*$^{-/-}$ mice: the non-fasted plasma glucose concentration tended to be only slightly elevated (P = 0.07) whereas plasma insulin was lower (P < 0.01) in β-*Tfb2m*$^{+/-}$ mice at seven months of age (Figure S2c,d). In β-*Tfb2m*$^{+/-}$ mice subjected to an intravenous glucose tolerance test, the total area under the curve (AUC) for plasma glucose increased (P < 0.05) and the acute insulin response tended to be lower (P = 0.07; Figure S2e,f).

Upon stimulation with 16.7 mM glucose, the maximal decrease in TMRM fluorescence intensity was reduced by 64% in isolated β-*Tfb2m*$^{+/-}$ islets (P < 0.05, Figure S2g). The final step in mitochondrial metabolism is the production of ATP; we found that β-*Tfb2m*$^{+/-}$ islets contained increased basal levels of ATP (P = 0.05; Figure S2h). The ATP content, however, was lower in these islets in the glucose-stimulated state compared to control islets (P < 0.05; Figure S2i).

Insulin secretion in response to glucose (P < 0.001) and α-KIC (P = 0.05) was also reduced from β-*Tfb2m*$^{+/-}$ islets (Figure S2j). Contrary to β-*Tfb2m*$^{-/-}$ islets, the insulin response to KCl was significantly decreased in β-*Tfb2m*$^{+/-}$ islets (Figure S2j; P < 0.001), but islet insulin content was not different (Control: 15.0 ± 3.4 μg/islet vs. β-*Tfb2m*$^{+/-}$: 18.6 ± 3.9 μg/islet). We found, however, that β-*Tfb2m*$^{+/-}$ mice had decreased pancreatic insulin content per weight of pancreas (P < 0.05; Figure S2k). This could be explained by reduced β-cell mass, i.e., reduced islet number since islet insulin content was unchanged. This finding is reminiscent of the reduction in islet density that was observed in β-*Tfb2m*$^{-/-}$ mice (Figure S1c). Thus, β-cell specific loss of *Tfb2m* expression from one allele is sufficient to impair both mitochondrial function and insulin secretion *in vivo* and *in vitro*.

3.8. Silencing of *TFB2M* in insulin-producing cells results in decreased expression of mitochondrial encoded genes, mitochondrial dysfunction and impaired insulin secretion

To reach deeper mechanistic understanding, we created an *in vitro* model of *TFB2M*-deficiency in INS-1 832/13 clonal cells, which, like β-

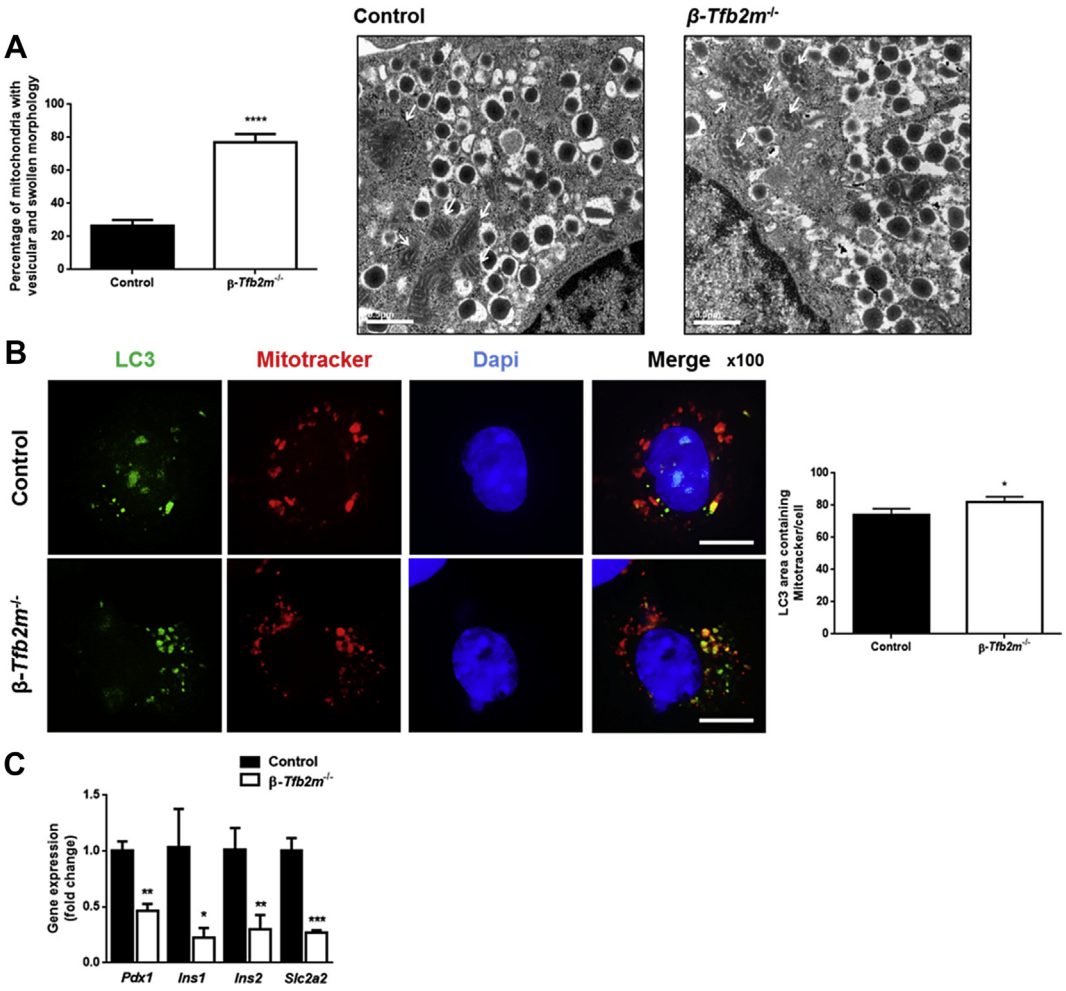

Figure 4: Loss of *Tfb2m* in β-cells leads to altered mitochondrial ultrastructure and impaired mitophagy. (A) Graph showing percentage of mitochondria with vesicular and swollen morphology in β-cells from control and β-*Tfb2m*$^{-/-}$ islets isolated from mice at 18 days of age. Representative electron micrograph showing normally shaped mitochondria in a control β-cell and vesicular and swollen mitochondria in β-*Tfb2m*$^{-/-}$ β-cell; control, *n*=34 images (4 mice), β-*Tfb2m*$^{-/-}$, *n* = 40 images (3 mice). White arrows point to mitochondria. Scale bars: 0.5 μm. (B) Left – Representative fluorescence microscopy image of cells expressing LC3-GFP (green) from dispersed control and β-*Tfb2m*$^{-/-}$ islets after treatment with Mitotracker (red). Nucleus stained with DAPI (blue). Scale bars, 10 μm. Right – Quantification of LC3^{+} area co-localized with Mitotracker in control and β-*Tfb2m*$^{-/-}$ islets; control and β-*Tfb2m*$^{-/-}$, 200 cells per condition was counted, *n* = 4 mice each at 18 days of age. (C) qRT-PCR analysis of *Pdx1*, *Ins1*, *Ins2*, and *Slc2a2* mRNA in islets from control and β-*Tfb2m*$^{-/-}$ mice, *n* = 3 mice. Data are mean ± s.e.m. Statistical differences were examined by unpaired Student's *t*-test. *P < 0.05, **P < 0.01, ***P < 0.001 and ****P < 0.0001 versus the corresponding value for control mice.

Tfb2m$^{-/-}$ mice, exhibited impaired insulin secretion (See Figure S3 for detailed data).

This model allowed us to determine O_2 consumption by cytochrome C oxidase (Complex IV), which is commonly used to assess mitochondrial respiratory chain activity and OXPHOS, thereby reflecting mitochondrial function [11]. Control INS-1 832/13 cells showed a progressive increase in oxygen consumption rate (OCR) following a rise in glucose concentration from 2.8 to 16.7 mM (Figure 6A). In contrast, not only did *TFB2M*-deficient cells exhibit lower basal OCR compared to controls, these cells also failed to increase their OCR to the same extent in response to glucose (Figure 6A). Upon addition of oligomycin, blocking ATP synthase and hence reflecting ATP turnover, OCR was decreased to a lesser extent in *TFB2M*-deficient cells; there was also a trend (P = 0.06) toward decreased H^{+} leak between control and *TFB2M*-deficient cells after correction for non-mitochondrial respiration (Figure 6A). In agreement with reduced ATP turnover (oligomycin-responsive OCR), the cellular ATP content after a 1 h incubation at 16.7 mM glucose was significantly reduced (P < 0.05) in *TFB2M*-deficient cells (Figure 6B). Taken together, our findings in *TFB2M*-silenced cells further reflect those of *Tfb2m*-deficient islets, i.e., mitochondrial dysfunction and impaired insulin secretion.

3.9. Silencing of *TFB2M* in insulin-producing cells results in impaired autophagy

We used *TFB2M*-deficient cells to understand whether impaired autophagy and mitophagy observed in β-*Tfb2m*$^{-/-}$ islets were caused by decreased *Tfb2m* expression *per se* and not a consequence of hyperglycemia and the prevailing pathophysiological condition. As in β-*Tfb2m*$^{-/-}$ islets, LC3^{+} puncta were more abundant (P < 0.0001; Figure S4a). Expression of *BECN1*, involved in early-stage autophagy, was increased in *TFB2M*-deficient cells (P < 0.01; Figure S4b). Expression of *CTSB* was increased (P < 0.001) whereas expression of *LAMP2* was unchanged (Figure S4b). Nevertheless, like β-*Tfb2m*$^{-/-}$ islets, autophagosome-lysosome fusion was disrupted in *TFB2M*-deficient cells (measured by LC3^{+} puncta co-stained with Lysotracker) (P < 0.01; Figure S4c). There was no effect of *TFB2M*-deficiency in

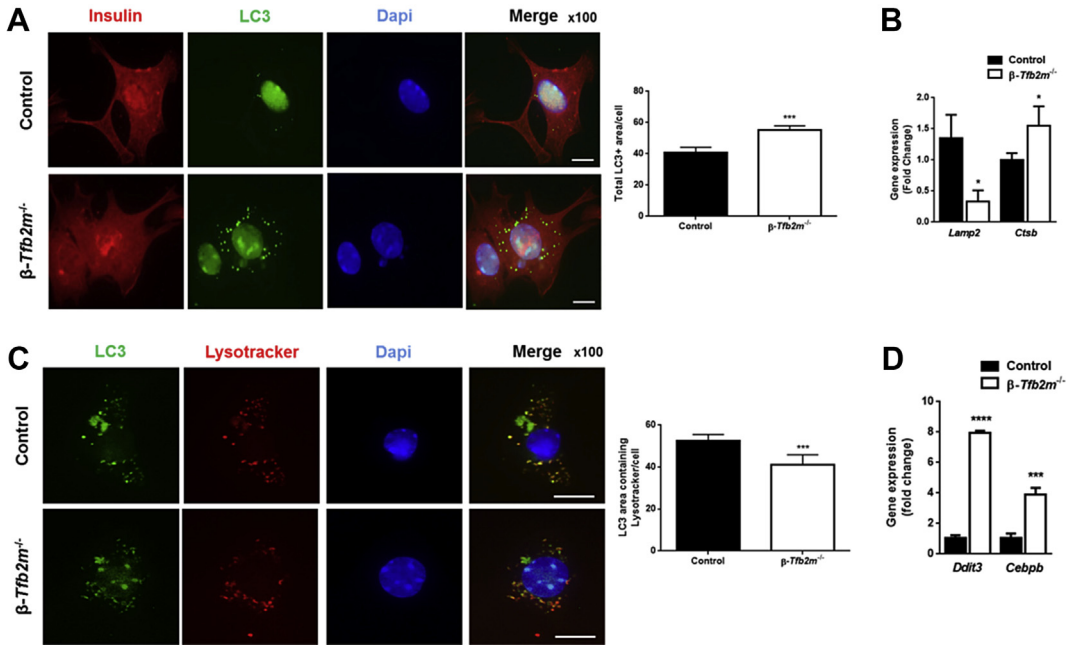

Figure 5: Loss of *Tfb2m* in β-cells leads to altered insulin ultrastructure and impaired autophagy. (A) Left — Representative fluorescence microscopy image of β-cells (stained for insulin — red) from control and β-*Tfb2m*$^{-/-}$ islets expressing LC3-GFP (green). Nucleus stained with DAPI (blue). Scale bars, 10 μm. Right — Quantification of total LC3^{+} area in control and β-*Tfb2m*$^{-/-}$ islets; control and β-*Tfb2m*$^{-/-}$, $n = 4$ mice each at 18 days of age. (B) qRT-PCR analysis of *Lamp2* and *Ctsb* mRNA in islets from control and β-*Tfb2m*$^{-/-}$ mice, $n = 3$ mice. (C) Left — Representative fluorescence microscopy image of cells expressing LC3-GFP (green) from control and β-*Tfb2m*$^{-/-}$ islets after treatment with Lysotracker (red). Nucleus stained with DAPI (blue). Scale bars, 10 μm. Right — Quantification of LC3^{+} area co-localized with Lysotracker in control and β-*Tfb2m*$^{-/-}$ islets; control and β-*Tfb2m*$^{-/-}$, $n = 4$ mice each at 18 days of age. (D) qRT-PCR analysis of *Ddit3* and *Cebpb* mRNA in islets from control and β-*Tfb2m*$^{-/-}$ mice, $n = 3$ mice. All data are mean ± s.e.m. Statistical differences were examined by unpaired Student's *t*-test. *P < 0.05, ***P < 0.001 and ****P < 0.0001 versus the corresponding value for control mice.

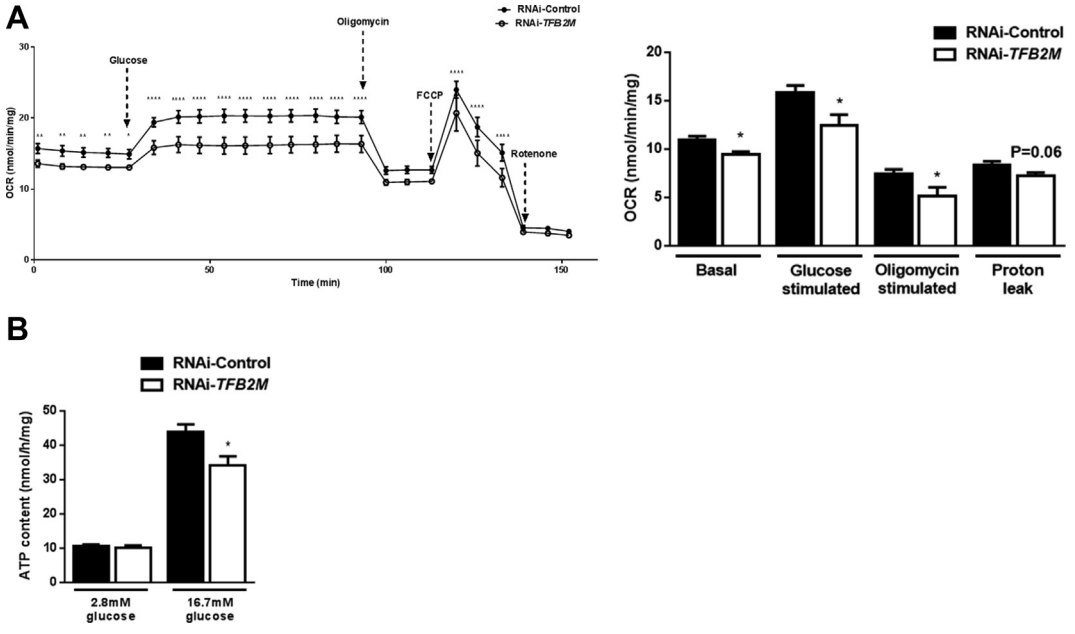

Figure 6: Silencing of *TFB2M* in insulin-producing cells results in impaired cellular respiration and decreased ATP content. (A) Left — Oxygen consumption rate (OCR) in control and *TFB2M*-deficient INS-1 832/13 clonal cells following treatment with glucose, oligomycin, rotenone, and carbonyl cyanide-4-(trifluoromethoxy) phenylhydrazone (FCCP). Right — Calculation of basal, glucose-stimulated and oligomycin-stimulated respiration as well as proton leak in control and *TFB2M*-deficient INS-1 832/13 clonal cells; $n = 5$ different cell passages/group. (B) ATP content at 2.8 mM glucose and upon stimulation with 16.7 mM glucose in control and *TFB2M*-deficient INS-1 832/13 clonal cells; $n = 9$ different cell passages/group. All data are mean ± s.e.m. Statistical differences were examined by unpaired Student's *t*-test or by a two-way repeated measures ANOVA followed by Tukey's post-hoc test (A — left) *P < 0.05, **P < 0.01, ***P < 0.001 and ****P < 0.0001 versus the corresponding value for controls.

INS-1 832/13 cells on expression of *CEBPB* mRNA (Figure S4d). However, there was increased expression of *DDIT3* ($P < 0.01$; Figure S4d). Thus, experimentally induced *TFB2M*-deficiency *in vitro* recapitulates impaired autophagy observed in β-*Tfb2m*$^{-/-}$ islets.

3.10. Silencing of *TFB2M* in insulin-producing cells results in disruption of the mitochondrial unfolded protein response and impaired mitophagy

DDIT3 also regulates the mitochondrial unfolded protein response (UPRmt), which is activated in response to mitochondrial stress upstream of the mitophagy pathway [27]. Indeed, protein abundance of the chaperone HSP60, which is typically activated as part of the UPRmt, was increased in *TFB2M*-deficient cells [$P < 0.01$; Figure S5a (left-hand panel)]. In contrast, gene expression of *HSP60* ($P < 0.001$) and the mitochondrial protease *CLPP* ($P < 0.01$) was reduced in these cells [Figure S5a (right-hand panel)].

Next, we examined mitophagy in *TFB2M*-silenced INS-1 832/13 cells. Indeed, these cells showed an increased number of LC3^{+} puncta co-stained with Mitotracker ($P < 0.0001$; Figure S5b). There was no change in PINK1 and PARKIN protein abundance (Figure S5c). Like β-*Tfb2m*$^{-/-}$ islets, *TFB2M*-deficient INS-1 832/13 cells displayed decreased expression of *PDX1* ($P < 0.05$) and its downstream targets, *INS1* ($P < 0.01$), *INS2* ($P < 0.05$), *SLC2A2* ($P < 0.01$) (Figure S5d), and *TFAM* ($P < 0.05$; Figure S3b). Taken together, *TFB2M*-deficiency in insulin-producing cells had a similar impact on mitophagy as in β-*Tfb2m*$^{-/-}$ islets.

3.11. Silencing of *TFB2M* in insulin-producing cells results in increased activation of apoptosis via the mitochondrial-dependent pathway

Seeing as both dysregulated autophagy and mitophagy are eventually likely to lead to increased apoptosis in β-cells, we assessed apoptotic markers. As in β-*Tfb2m*$^{-/-}$ islets, we found increased activation of the apoptotic pathway in *TFB2M*-deficient INS-1 832/13 cells, indicated by increased abundance of cleaved caspase-3 ($P < 0.05$; Figure 7A). Expression of the pro-apoptotic protein BAX ($P < 0.01$; Figure 7A) was induced but also of the anti-apoptotic BCL-2, as well as the serine/threonine kinase AKT and phosphorylated-AKT (Ser 473) ($P < 0.05$; Figure 7B).

3.12. Silencing of *TFB2M* in insulin-producing cells results in increased production of reactive oxygen species (ROS)

Reduced *PDX1* expression, as observed in this study, under certain conditions, may result from increased ROS [28]. Indeed, silencing of *TFB2M* resulted in increased levels of ROS at both 2.8 and 16.7 mM glucose ($P < 0.05$; Figure 8A,B). Treatment of *TFB2M*-deficient cells

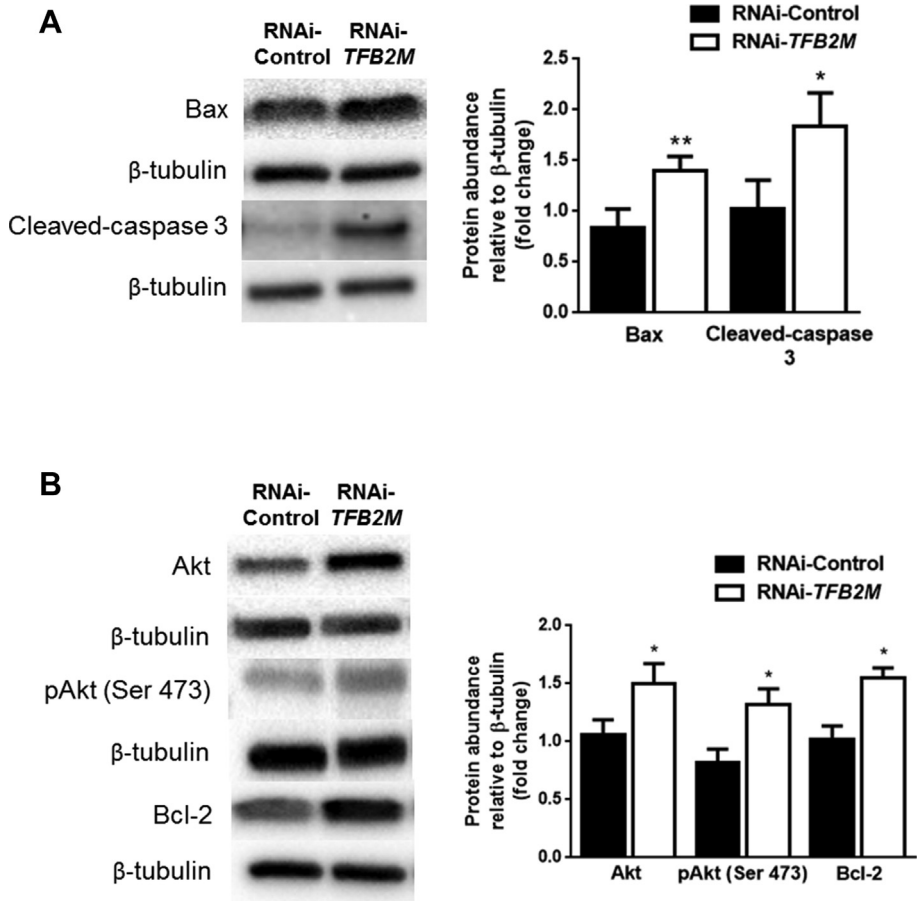

Figure 7: Silencing of *TFB2M* in insulin-producing cells results in increased activation of apoptosis via the mitochondrial-dependent pathway. (A) Western blot and densitometry analysis of BAX and Cleaved-caspase 3 protein abundance in control and *TFB2M*-deficient INS-1 832/13 clonal cells; $n = 5$ different cell passages/group. (B) Western blot and densitometry analysis of AKT, phospho-AKT (Ser 473), and BCL-2 protein abundance in control and *TFB2M*-deficient INS-1 832/13 clonal cells; $n = 5$ different cell passages/group. Representative images for quantitative western blots are shown. Statistical differences were examined by unpaired Student's *t*-test. *$P < 0.05$ and **$P < 0.01$ versus the corresponding value for controls.

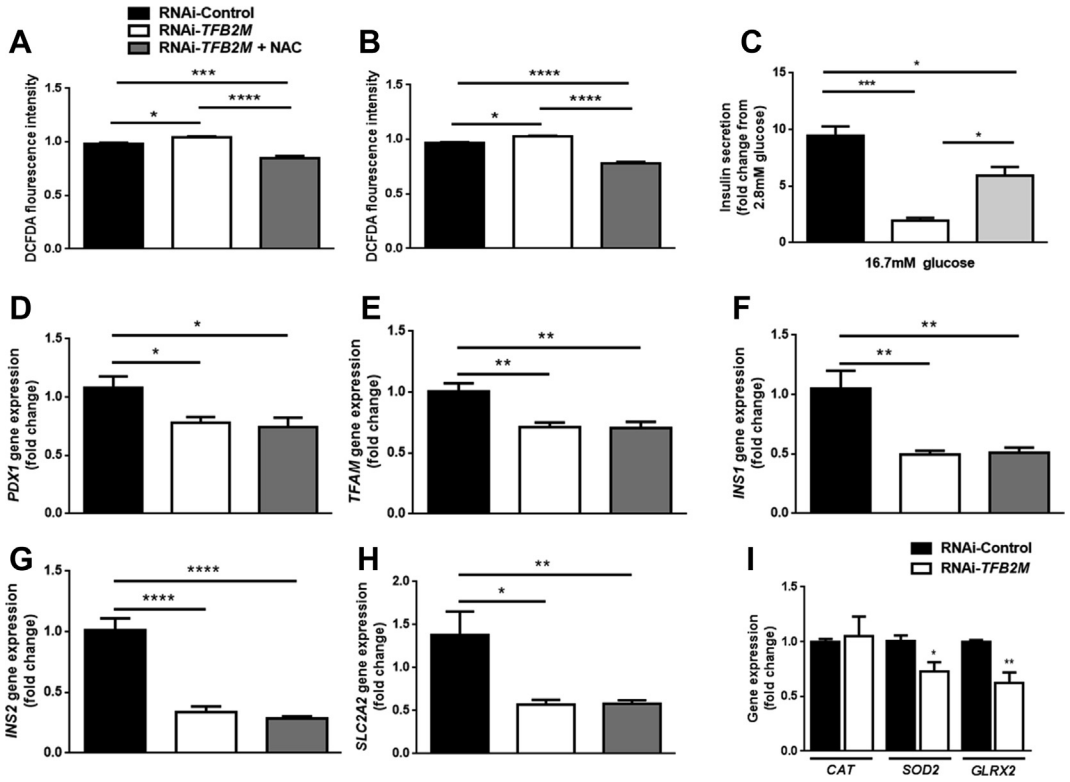

Figure 8: Silencing of *TFB2M* in insulin-producing cells results in increased production of reactive oxygen species (ROS). Quantification of ROS using the fluorogenic dye 2′,7′ −dichlorofluorescin diacetate (DCFDA) in control and *TFB2M*-deficient INS-1 832/13 clonal cells in the presence and absence of 10 μM of N-acetyl-L-cysteine (NAC) at 2.8 mM (A) and 16.7 mM (B) glucose. (C) Insulin secretion from control and *TFB2M*-deficient INS-1 832/13 clonal cells in the presence and absence of 10 μM NAC that were incubated for 1 h in 2.8 mM and 16.7 mM glucose. (D—H) qRT-PCR analysis of *PDX1*, *TFAM*, *INS1*, *INS2*, and *SLC2A2* mRNA in control and *TFB2M*-deficient INS-1 832/13 clonal cells in the presence and absence of 10 μM NAC. (I) qRT-PCR analysis of *CAT*, *SOD2*, and *GLRX2* mRNA in control and *TFB2M*-deficient INS-1 832/13 clonal cells; $n = 5$ different cell passages/group. Statistical differences were examined by a one-way ANOVA followed by Tukey's post-hoc test (A—H) or by unpaired Student's *t*-test (I). *P $<$ 0.05, **P $<$ 0.01, ***P $<$ 0.001 and ****P $<$ 0.0001 versus the corresponding value for controls.

with the antioxidant N-acetyl cysteine (NAC) reduced ROS levels at both 2.8 mM and 16.7 mM glucose (P $<$ 0.0001; Figure 8A,B). The ROS level in *TFB2M*-deficient cells treated with NAC also remained lower than in control cells at 2.8 (P $<$ 0.001) and 16.7 mM glucose (P $<$ 0.0001; Figure 8A,B).

Treatment of *TFB2M*-deficient cells with NAC also improved GSIS (P $<$ 0.05; Figure 8C), but hormone secretion was still lower than in control cells (P $<$ 0.05; Figure 8C). Despite the reduction of ROS levels in *TFB2M*-deficient cells by NAC, treatment with this antioxidant was unable to ablate the decrease in gene expression of *PDX1* (P $<$ 0.05) and its downstream targets *TFAM* (P $<$ 0.01), *INS1* (P $<$ 0.01), *INS2* (P $<$ 0.0001), and *SLC2A2* (P $<$ 0.01) (Figure 8D—H). Since *TFB2M*-deficiency resulted in increased ROS levels, we investigated the expression of key antioxidant enzymes, which play a role in the defense against ROS. Expression of *CAT* was unchanged but that of *SOD2* (P $<$ 0.05) and *GLRX2* (P $<$ 0.01) was decreased in *TFB2M*-deficient INS-1 832/13 cells (Figure 8I).

4. DISCUSSION

TFB2M plays an important role in transcription of mtDNA through its primary role in melting the promoter, as well as stabilizing the open promoter complex [8,29]. To date, the importance of TFB2M in mitochondrial and cellular function and implications thereof for pancreatic β-cells, which depend on mitochondria for control of insulin secretion and β-cell mass, remain unknown. The current study explored the role of this mitochondrial transcription factor in β-cell function and outlined possible molecular mechanism(s) underpinning disrupted mitochondrial metabolism and β-cell dysfunction, which may lead to T2D. Here, we used three different experimental models of *Tfb2m*-deficiency in β-cells. We found that loss of *Tfb2m* resulted in decreased expression of mitochondrial-encoded genes, as well as reduced mtDNA content. This led to severe mitochondrial dysfunction, characterized by diminished hyperpolarization of the inner mitochondrial membrane, impaired oxygen consumption, and reduced ATP production. Together, this resulted in perturbed stimulus-secretion coupling in β-cells, thereby leading to impaired insulin secretion and, subsequently, progressive hyperglycemia in mice.

A striking result of this study was how rapidly these perturbations evolved in *Tfb2m*-deficient mice compared to those previously seen in mice with a β-cell specific loss of either *Tfam* [10] or *Tfb1m* [12]. At seven weeks of age, *Tfam*-deficient mice display perturbed mtDNA expression and consequently severe respiratory chain deficiency in pancreatic β-cells. Loss of insulin-producing β-cells, however, was detected when mice are 39 weeks old [10]. In *Tfb1m*-deficient mice, mitochondrial dysfunction is apparent at three months of age followed by hyperglycemia, which is first evident at four months of age [12]. In contrast, the pathological changes observed here in *Tfb2m*-deficient mice occurred at the earliest time point studied (day 18), a time point when these mice were only slightly hyperglycemic in the non-fasted state. Since plasma insulin concentration was not reduced in β-*Tfb2m*$^{-/-}$ mice at this age, we speculate that β-cell mass is still

intact. Indeed, mice ingest a carbohydrate-poor diet prior to weaning, requiring little insulin, which may explain the moderate hyperglycemia and preserved β-cell mass. Over time, loss of β-cell mass became apparent also in β-*Tfb2m*$^{-/-}$ mice (seven weeks of age). At this point, β-cell function was severely compromised with a more than 2-fold elevation of plasma glucose concentration and a 75% reduction in plasma insulin concentration.

The effect of gene dosage on *Tfb2m* expression and the resulting delayed phenotype in β-*Tfb2m*$^{+/-}$ mice were other important findings. Signs of β-cell dysfunction at around six months of age were evident as decreased plasma insulin concentration in the non-fasted state, as well as retarded glucose elimination and a tendency toward impaired acute insulin response during an IVGTT. This may be attributed to a reduction of β-cell mass at this age. Loss of one functional *Tfb2m* allele also resulted in mitochondrial dysfunction and consequently impaired insulin secretion from β-cells. Furthermore, islets from β-*Tfb2m*$^{+/-}$ mice displayed impaired insulin exocytotic capacity, which was not present in *Tfb2m*$^{-/-}$ mice. We believe that this difference is due to the additional effect of aging; β-*Tfb2m*$^{+/-}$ islets were isolated from six month old mice versus that of young 18 and 35-day old *Tfb2m*$^{-/-}$ mice.

Functional β-cell mass is determined both by robust stimulus-secretion coupling and the number of β-cells. Mitochondrial dysfunction, therefore, will have a huge impact on both these parameters. Indeed, both the homozygous and heterozygous *Tfb2m*-deficient mice displayed impaired stimulus-secretion coupling and reduced β-cell mass. While it is clear how mitochondrial dysfunction impairs stimulus-secretion coupling, the pathways that lead from mitochondrial dysfunction to loss of β-cell mass are less well understood. Proper control of autophagic processes is essential for the maintenance of normal β-cell architecture and, hence, β-cell mass [25]. We, therefore, sought to determine whether autophagy is impaired upon *Tfb2m*-deficiency. There was increased expression of the later-stage autophagy marker *Ctsb* [24] along with decreased expression of *Lamp2*, which is a negative regulator of autophagy [25]. This was accompanied by increased activation of the autophagic machinery. The maturation and degradation of the autophagosome, which involve fusion with the endosome—lysosome to form autolysosomes [30], is a critical stage of autophagy. This process was disrupted, however, upon *Tfb2m*-deficiency, suggesting that although a mechanism or mechanisms were activated within *Tfb2m*-deficient cells to increase autophagic clearance, i.e., of insulin secretory granules, autophagy was still impaired. Importantly, this could lead to accumulation of autophagic vacuoles in the cytoplasm and autophagic cell death distinct from apoptosis [31]. Indeed, LC3-labeled vacuoles have been shown to accumulate in cells lacking *Lamp2* expression but co-localization of LC3 and lysosomes to decrease, suggesting that fusion between autophagic vacuoles and lysosomes is inhibited [31]. Autophagy is also activated in response to ER stress [26]. Indeed, we found increased expression of the ER stress markers *DDIT3* and *CEBPB* [32].

The first line of defense against mitochondrial stress or dysfunction is the UPRmt, which is activated before mitophagy ensues [27]. UPRmt is triggered by depletion of mtDNA and/or mutations reducing expression of components of the respiratory chain or perturbing their ability to fold [27,33]. In *TFB2M*-deficient INS-1 832/13 cells, we found increased gene expression of *DDIT3*, which regulates UPRmt by activating transcription of mitochondrial chaperones and proteases [34], along with a corresponding increase in abundance of the chaperone HSP60 but not the mitochondrial protease CLPP. Upregulation of both HSP60 and CLPP reduces mitochondrial protein aggregation [35]. Furthermore, CLPP, which is localized within the mitochondrial matrix, serves as a sensor of unfolded proteins [36]. This implies, therefore, that an upregulation of HSP60 alone in *TFB2M*-deficient INS-1 832/13 cells reflects an insufficient capacity of these cells to mount an appropriate UPRmt. Interestingly, the gene expression of the DDIT3 target *CLPP* and its target *HSP60* was reduced in *TFB2M*-deficient cells. This has previously been shown to perturb mitochondrial morphology [37]. Indeed, *Tfb2m*-deficiency in mouse β-cells resulted in increased abundance of vesicular and swollen mitochondria. Mitochondrial inner membrane conformation changes to the vesicular form during Cytochrome C release, and the matrix swells during or after the loss of mitochondrial membrane potential [38]. Taken together, these results suggest that *TFB2M*-deficient cells may be trying to mount a UPRmt (as reflected by increased DDIT3 and HSP60), but the reduction in *CLPP* and/or *HSP60* gene expression may be a sign of "weakness" in the system. This could lead to the UPRmt system being overwhelmed, resulting instead in activation of mitophagy [27]. Indeed, the increased number of mitochondria targeted to LC3-positive vesicles, observed in *Tfb2m*-deficient β-cells, indicated either an increased flux through mitophagy or impaired autophagosome-lysosome fusion, i.e., incomplete mitophagy flux [22]. The lack of any major changes in expression of genes and proteins involved in mitophagy supports the notion that mitophagy flux in *Tfb2m*-deficient β-cells is impaired.

UPRmt, ER stress, mitophagy, and autophagy in β-cells ultimately converge on activation of apoptotic pathways. Indeed, we observed activation of apoptosis via the mitochondrial-dependent pathway. This was reflected by higher levels of pro-apoptotic Bax and Cleaved-caspase 3 in *TFB2M*-deficient β-cells. Signs of compensatory mechanisms in *TFB2M*-deficient cells suggest that they are struggling to cope with increased activation of the apoptotic pathway, as evidenced by up-regulation of AKT and its anti-apoptotic target BCL-2 [40].

Oxidative stress and/or ROS are frequently associated with mitochondrial dysfunction as well as cell death. In β-cells, the generation of ROS is coupled to glycolytic and respiratory metabolism [41]. Antioxidant enzymes contained within cells are the first line of defense against excessive ROS levels [42]. These antioxidant enzymes are expressed at comparatively low levels in β-cells, rendering them more susceptible to oxidative stress [28]. We have previously reported a link between ROS generation and cell death in *Tfb1m*-deficient islets [12]. Here, we found that mitochondrial dysfunction in *TFB2M*-deficient INS-1 832/13 cells was associated with increased ROS levels. These cells also exhibited impaired antioxidant defense, indicated by decreased expression of *SOD2* and *GLRX2*. Treatment with the antioxidant NAC was able to normalize ROS levels as well as to slightly improve insulin secretion.

The pancreatic homeodomain transcription factor PDX1 is a master regulator of the β-cell, important for its embryonic development and differentiated function [43]. Heterozygous mutations in *PDX1* are associated with T2D in humans [44]. Amongst the roles of PDX1 is its ability to activate transcription of *TFAM* by binding to its promoter [43] as well as regulation of autophagosome-lysosome fusion, autophagy, and mitophagy [22,45]. Moreover, PDX1 also affects insulin production and secretion via its target genes *Ins1* and *Ins2*. Loss of *Pdx1* has been shown to lead to increased apoptosis in β-cells. In this study, we found that *Tfb2m*-deficiency resulted in decreased expression of *Pdx1* and a number of its downstream targets. These results suggest that PDX1 may serve as a common factor mediating the observed changes in *Tfb2m*-deficient cells. ROS have been shown to affect the expression and function of *Pdx1* at epigenetic, transcriptional, and post-translational levels [28]. In this study, we found both increased ROS levels and decreased *Pdx1* expression, raising the possibility that ROS

is the major determinant of the pathological changes observed. Although treatment with NAC was able to normalize ROS levels, the expression of *PDX1* and its targets remained decreased in NAC-treated *TFB2M*-deficient cells. This suggests that increased ROS levels provide only a partial explanation, linking loss of *TFB2M*, mitochondrial dysfunction, and, consequently, impaired insulin secretion.

5. CONCLUSION

We employed three different models of *Tfb2m*-deficiency — homozygous and heterozygous β-cell knock out in mouse and RNAi in clonal insulin-producing cells — to identify an important role of TFB2M in β-cell function. Specifically, we have outlined molecular mechanisms that operate during *Tfb2m*-deficiency and mitochondrial dysfunction. Importantly, we found that, in some instances, perturbation of β-cell metabolism leads to activation of compensatory mechanisms limiting cellular dysfunction and damage. Ultimately, however, widespread mitochondrial dysfunction overwhelms cell-protective systems, such as UPRmt, autophagy, and mitophagy, leading to β-cell dysfunction as well as increased apoptosis and loss of β-cell mass. The rapid onset and dramatic consequences of TFB2M-deficiency suggest an unforeseen and critical role for this mitochondrial transcription factor.

AUTHOR CONTRIBUTIONS

LMN and BV performed most experiments, analyzed data and wrote the manuscript. AM, LA MA, DJ, and IGM performed experiments and analyzed data. MF, LE, and NW provided feedback on data interpretation. HM conceived the project and wrote the manuscript. All authors reviewed the manuscript.

ACKNOWLEDGEMENTS

The authors thank Nils-Göran Larsson (Karolinska Institute, Sweden) for constructive feedback on the manuscript. Laila Jacobsson is acknowledged for genotyping the mice. Ann-Helen Thorén Fischer is acknowledged for her assistance with animal work. Financial support was received from the Medical Faculty at Lund University, Swedish Diabetes Foundation, Albert Påhlsson Foundation, Swedish Research Council, Diabetes Wellness, and the Swedish Foundation for Strategic Research.

CONFLICT OF INTERESTS

The authors have no competing interests to declare.

APPENDIX A. SUPPLEMENTARY DATA

Supplementary data related to this article can be found at http://dx.doi.org/10.1016/j.molmet.2017.05.005.

REFERENCES

[1] Lowell, B.B., Shulman, G.I., 2005. Mitochondrial dysfunction and type 2 diabetes. Science 307(5708):384—387.
[2] Thomsen, S.K., Gloyn, A.L., 2014. The pancreatic beta cell: recent insights from human genetics. Trends in Endocrinology and Metabolism 25(8):425—434.
[3] Aguiree, F., Brown, A., Cho, N.H., Dahlquist, G., Dodd, S., Dunning, T., et al., 2013. IDF diabetes atlas, 6th ed., vol. 155. Basel, Switzerland: International Diabetes Federation.
[4] Ardestani, A., Paroni, F., Azizi, Z., Kaur, S., Khobragade, V., Yuan, T., et al., 2014. MST1 is a novel regulator of apoptosis in pancreatic beta-cells. Nature Medicine 20(4):385—397.
[5] Supale, S., Li, N., Brun, T., Maechler, P., 2012. Mitochondrial dysfunction in pancreatic β cells. Trends in Endocrinology and Metabolism 23(9):477—487.
[6] Maechler, P., Li, N., Casimir, M., Vetterli, L., Frigerio, F., Brun, T., 2010. Role of mitochondria in beta-cell function and dysfunction. Advances in Experimental Medicine and Biology 654:193—216.
[7] Maechler, P., Wollheim, C.B., 2001. Mitochondrial function in normal and diabetic [beta]-cells. Nature 414(6865):807—812.
[8] Litonin, D., Sologub, M., Shi, Y., Savkina, M., Anikin, M., Falkenberg, M., et al., 2010. Human mitochondrial transcription revisited: only TFAM and TFB2M are required for transcription of the mitochondrial genes in vitro. Journal of Biological Chemistry 285(24):18129—18133.
[9] Metodiev, M., Lesko, N., Park, C.B., Cámara, Y., Shi, Y., Wibom, R., et al., 2009. Methylation of 12S rRNA is necessary for in vivo stability of the small subunit of the mammalian mitochondrial ribosome. Cell Metabolism 9:1—12.
[10] Silva, J.P., Kohler, M., Graff, C., Oldfors, A., Magnuson, M.A., Berggren, P.O., et al., 2000. Impaired insulin secretion and beta-cell loss in tissue-specific knockout mice with mitochondrial diabetes. Nature Genetics 26(3):336—340.
[11] Koeck, T., Olsson, A.H., Nitert, M.D., Sharoyko, V.V., Ladenvall, C., Kotova, O., et al., 2011. A common variant in TFB1M is associated with reduced insulin secretion and increased future risk of type 2 diabetes. Cell Metabolism 13(1):80—91.
[12] Sharoyko, V.V., Abels, M., Sun, J., Nicholas, L.M., Mollet, I.G., Stamenkovic, J.A., et al., 2014. Loss of TFB1M results in mitochondrial dysfunction that leads to impaired insulin secretion and diabetes. Human Molecular Genetics.
[13] Herrera, P.L., 2000. Adult insulin- and glucagon-producing cells differentiate from two independent cell lineages. Development 127(11):2317—2322.
[15] Fex, M., Wierup, N., Nitert, M.D., Ristow, M., Mulder, H., 2007. Rat insulin promoter 2-Cre recombinase mice bred onto a pure C57BL/6J background exhibit unaltered glucose tolerance. Journal of Endocrinology 194(3):551—555.
[16] Goehring, I., Sharoyko, V.V., Malmgren, S., Andersson, L.E., Spegel, P., Nicholls, D.G., et al., 2014. Chronic high glucose and pyruvate levels differentially affect mitochondrial bioenergetics and fuel-stimulated insulin secretion from clonal INS-1 832/13 cells. Journal of Biological Chemistry 289(6):3786—3798.
[17] Kong, M., Bhattacharya, R.N., James, C., Basu, A., 2005. A statistical approach to estimate the 3D size distribution of spheres from 2D size distributions. Geological Society of America Bulletin 117(1—2):244—249.
[18] Dehoff, R.T., Rhines, F.N., 1961. Determination of the number of particles per unit volume from measurements made on random plane sections: the general cylinder and the ellipsoid. Transactions of the Metallurgical Society of AIME 221:975—982.
[19] Hohmeier, H.E., Mulder, H., Chen, G., Henkel-Rieger, R., Prentki, M., Newgard, C.B., 2000. Isolation of INS-1-derived cell lines with robust ATP-sensitive K+ channel-dependent and -independent glucose-stimulated insulin secretion. Diabetes 49(3):424—430.
[20] Kuznetsov, A.V., Gnaiger, E., 2010. Laboratory protocol complex I (NADH: Ubiquinone Oxidoreductase; EC 1.6. 5.3) mitochondrial membrane.
[21] Malmgren, S., Nicholls, D.G., Taneera, J., Bacos, K., Koeck, T., Tamaddon, A., et al., 2009. Tight coupling between glucose and mitochondrial metabolism in clonal beta-cells is required for robust insulin secretion. Journal of Biological Chemistry 284(47):32395—32404.
[22] Soleimanpour, S.A., Ferrari, A.M., Raum, J.C., Groff, D.N., Yang, J., Kaufman, B.A., et al., 2015. Diabetes susceptibility genes Pdx1 and Clec16a function in a pathway regulating mitophagy in beta-cells. Diabetes 64(10):3475—3484.

[23] Jin, S.M., Youle, R.J., 2012. PINK1- and Parkin-mediated mitophagy at a glance. Journal of Cell Science 125(Pt 4):795—799.
[24] Marsh, B.J., Soden, C., Alarcon, C., Wicksteed, B.L., Yaekura, K., Costin, A.J., et al., 2007. Regulated autophagy controls hormone content in secretory-deficient pancreatic endocrine beta-cells. Molecular Endocrinology 21(9): 2255—2269.
[25] Chen, Z.F., Li, Y.B., Han, J.Y., Wang, J., Yin, J.J., Li, J.B., et al., 2011. The double-edged effect of autophagy in pancreatic beta cells and diabetes. Autophagy 7(1):12—16.
[26] Ogata, M., Hino, S., Saito, A., Morikawa, K., Kondo, S., Kanemoto, S., et al., 2006. Autophagy is activated for cell survival after endoplasmic reticulum stress. Molecular and Cellular Biology 26(24):9220—9231.
[27] Pellegrino, M.W., Nargund, A.M., Haynes, C.M., 2013. Signaling the mitochondrial unfolded protein response. Biochimica et Biophysica Acta 1833(2): 410—416.
[28] Lei, X.G., Vatamaniuk, M.Z., 2011. Two tales of antioxidant enzymes on beta cells and diabetes. Antioxidants & Redox Signal 14(3):489—503.
[29] Sologub, M., Litonin, D., Anikin, M., Mustaev, A., Temiakov, D., 2009. TFB2 is a transient component of the catalytic site of the human mitochondrial RNA polymerase. Cell 139(5):934—944.
[30] Zhou, J., Tan, S.-H., Nicolas, V., Bauvy, C., Yang, N.-D., Zhang, J., et al., 2013. Activation of lysosomal function in the course of autophagy via mTORC1 suppression and autophagosome-lysosome fusion. Cell Research 23(4):508—523.
[31] Gonzalez-Polo, R.A., Boya, P., Pauleau, A.L., Jalil, A., Larochette, N., Souquere, S., et al., 2005. The apoptosis/autophagy paradox: autophagic vacuolization before apoptotic death. Journal of Cell Science 118(Pt 14): 3091—3102.
[32] Bartolome, A., Kimura-Koyanagi, M., Asahara, S., Guillen, C., Inoue, H., Teruyama, K., et al., 2014. Pancreatic beta-cell failure mediated by mTORC1 hyperactivity and autophagic impairment. Diabetes 63(9):2996—3008.
[33] Suen, D.F., Narendra, D.P., Tanaka, A., Manfredi, G., Youle, R.J., 2010. Parkin overexpression selects against a deleterious mtDNA mutation in heteroplasmic cybrid cells. Proceedings of the National Academy of Sciences of the United States of America 107(26):11835—11840.
[34] Papa, L., Germain, D., 2014. SirT3 regulates the mitochondrial unfolded protein response. Molecular and Cellular Biology 34(4):699—710.
[35] Zhao, Q., Wang, J., Levichkin, I.V., Stasinopoulos, S., Ryan, M.T., Hoogenraad, N.J., et al., 2002. A mitochondrial specific stress response in mammalian cells. EMBO Journal 21(17):4411—4419.
[36] Haynes, C.M., Ron, D., 2010. The mitochondrial UPR — protecting organelle protein homeostasis. Journal of Cell Science 123(Pt 22):3849—3855.
[37] Haynes, C.M., Petrova, K., Benedetti, C., Yang, Y., Ron, D., 2007. ClpP mediates activation of a mitochondrial unfolded protein response in *C. elegans*. Developmental Cell 13(4):467—480.
[38] Sun, M.G., Williams, J., Munoz-Pinedo, C., Perkins, G.A., Brown, J.M., Ellisman, M.H., et al., 2007. Correlated three-dimensional light and electron microscopy reveals transformation of mitochondria during apoptosis. Nature Cell Biology 9(9):1057—1065.
[40] Majewski, N., Nogueira, V., Robey, R.B., Hay, N., 2004. Akt inhibits apoptosis downstream of BID cleavage via a glucose-dependent mechanism involving mitochondrial hexokinases. Molecular and Cellular Biology 24(2):730—740.
[41] Pi, J., Bai, Y., Zhang, Q., Wong, V., Floering, L.M., Daniel, K., et al., 2007. Reactive oxygen species as a signal in glucose-stimulated insulin secretion. Diabetes 56(7):1783—1791.
[42] Robertson, R.P., Harmon, J.S., 2007. Pancreatic islet beta-cell and oxidative stress: the importance of glutathione peroxidase. FEBS Letters 581(19):3743—3748.
[43] Gauthier, B.R., Wiederkehr, A., Baquie, M., Dai, C., Powers, A.C., Kerr-Conte, J., et al., 2009. PDX1 deficiency causes mitochondrial dysfunction and defective insulin secretion through TFAM suppression. Cell Metabolism 10(2):110—118.
[44] Stoffers, D.A., Ferrer, J., Clarke, W.L., Habener, J.F., 1997. Early-onset type-II diabetes mellitus (MODY4) linked to IPF1. Nature Genetics 17(2):138—139.
[45] Fujimoto, K., Hanson, P.T., Tran, H., Ford, E.L., Han, Z., Johnson, J.D., et al., 2009. Autophagy regulates pancreatic beta cell death in response to Pdx1 deficiency and nutrient deprivation. Journal of Biological Chemistry 284(40): 27664—27673.

